Collaborative Positioning for Formation Flight of Cargo Aircraft

Jason H. Rife, Tufts University

>> Accepted Article <<

CITATION:
Jason Rife. "Collaborative Positioning for Formation Flight of Cargo Aircraft", *Journal of Guidance, Control, and Dynamics*, Vol. 36, No. 1 (2013), pp. 304-307. https://doi.org/10.2514/1.55834.

CORRESPONDING AUTHOR:
Jason Rife
jason.rife@tufts.edu

FINANCIAL SUPPORT:
AFRL (Contract FA8650-11-M-3117) and prime contractor Physics, Materials, and Applied Mathematics, Inc.

Collaborative Positioning for Formation Flight

Jason Rife[1]

Tufts University, Medford, MA, 02155

A collaborative method is presented for fusing together ranging and bearing measurements to support formation flight when limited communication among aircraft is possible. Compared to more conventional Station Keeping Equipment (SKE) the new approach, called Collaborative Multi-Aircraft Positioning (CMAP), exploits measurement redundancy to improve overall positioning accuracy and infer clock biases when aircraft clocks have not been precisely synchronized in advance. The performance of the basic CMAP algorithm is further enhanced by the introduction of a filtering algorithm that mitigates sensitivity to large bearing measurement errors. Algorithm performance is evaluated using Monte Carlo simulations, which suggest that CMAP performance is sufficient to enable precision airdrop when bearing measurement error is as high as 10° one-sigma, even for aircraft separated over long distances (as far as 9 km).

I. Nomenclature

a_i = Barometric altimeter reading of aircraft i
b_{ij} = Clock error of aircraft i w.r.t. j
d_{ij} = Downward distance of aircraft i w.r.t. j
e_{ij} = Eastward distance of aircraft i w.r.t. j
h_{ij} = altitude difference of aircraft i w.r.t. j
$\mathbf{H}_{ij}$ = linear sensor model for aircraft i w.r.t. j
n_{ij} = Northward distance of aircraft i w.r.t. j

[1] Assistant Professor, Mechanical Engineering, 200 College Ave; jason.rife@tufts.edu.

$\mathbf{P}_f$ = error covariance of formation states
$\mathbf{P}_{ij}$ = error covariance of states of aircraft *i* w.r.t. *j*
r_{ij} = slant range of aircraft *i* from *j*
$\mathbf{R}_f$ = error covariance of shared formation sensor data
$\mathbf{R}_{ij}$ = error covariance of sensing of aircraft *i* w.r.t. *j*
$\mathbf{x}_f$ = vector of relative positions of all formation aircraft
$\mathbf{x}_{ij}$ = relative position vector to aircraft *i* w.r.t. *j*
$\mathbf{y}_f$ = vector of sensor data shared across formation
$\mathbf{y}_{ij}$ = vector of sensor measurements of *i* w.r.t. *j*
$\mathbf{W}$ = weighting matrix for $\mathbf{y}_f$
α_f = formation rigid-body rotation angle
α_{ij} = bearing angle of aircraft *i* w.r.t. *j*
$\varepsilon_{\mathbf{x},ij}$ = error of position estimate of *i* w.r.t. *j*
$\varepsilon_{\mathbf{y},ij}$ = error of measurements of *i* w.r.t. *j*
Φ = rotation matrix
ψ_i = yaw angle of aircraft *i*
ρ_{ij} = pseudo-range of aircraft *i* w.r.t. *j*

II. Introduction

THIS paper introduces a collaborative method for computing the relative positions of cargo aircraft in formation flight using range and bearing measurements communicated throughout the formation. The new method is compared to more conventional techniques, representative of those used in current-generation Station Keeping Equipment (SKE) for military cargo aircraft.

A capability for precise relative positioning of aircraft within a formation is critical for a number of applications. Typical formation-flight applications, such as precision airdrop of personnel and supplies by military cargo aircraft [1], require relative positioning with moderate accuracy (about 50 m, 95%). Accuracy requirements are higher (about 4m, 95%) to achieve drag reduction for civilian or military cargo aircraft formations [2]-[4]. Airborne refueling is an even more demanding application, with very aggressive positioning accuracy requirements (about 1m, 95%) [5]-[6]. The primary focus of this paper is the development of an enhanced relative-position estimation capability for precision airdrop; however, it is likely that the same methods might be extended to more aggressive applications in the future.

Existing relative-positioning systems that support precision airdrop can be categorized into two basic operational concepts: conventional SKE systems and GPS-based systems. Conventional SKE systems use radio signals (at approximately 3 GHz) to determine bearing and one-way range between aircraft pairs [7]. In existing SKE systems, slant ranging measurements are obtained by clocking the time-of-flight for a radio signal transmitted from an omnidirectional antenna. Rotating directional receiver antennas are used to infer the angle of arrival of the signal and, thereby, to determine the bearing angle between the transmitting and receiving aircraft. The relative position vector between the transmitting and receiving aircraft is reconstructed by combining the slant range and bearing measurements with barometric altimeter data.

The major limitation of conventional SKE systems is the ease with which a ground observer can detect the 3 GHz radio signal, even tens of kilometers away from the transmitting antennas [8]. The relative ease of detecting SKE transmissions means that an adversary may gain significant advance warning of a formation's approach.

To improve system accuracy and stealth, GPS-based alternatives to conventional SKE systems have emerged in the last decade. In such systems, each aircraft transmits its GPS position fix to other aircraft in the formation, either through using equipment compatible with the civilian Automatic Dependent Surveillance – Broadcast (ADS-B) standard [9] or using a proprietary communications standard [10], [11]. GPS-based relative positioning is more accurate than conventional SKE, with an accuracy tighter than 10 m (95%) for an ADS-B type system [12] and as tight as 30 cm (95%) for customized carrier-phase solutions with inertial integration [13]. Moreover, GPS-based relative positioning accuracy does not deteriorate when formation spacing is large, unlike conventional SKE, in which the reliance on bearing measurements causes accuracy to degrade in rough proportion to the distance between aircraft pairs. A GPS-based approach is also low-cost compared to conventional SKE, since avionics can be assembled from mass-produced component technologies.

The major liability of GPS-based relative positioning for formation flight is the ease with which Radio-Frequency Interference (RFI) can jam the GPS signal. The low signal strength of GPS satellite transmissions is a well-known vulnerability that threatens civilian and military systems alike [14]. Many technologies have been proposed to mitigate RFI jamming, such as the fusion of GPS with inertial sensing to coast through short GPS outages and the use of Controlled Reception Pattern Array (CRPA) antennas to boost signal strength and null jamming sources [15]. However, these technologies cannot ultimately guarantee uninterrupted navigation service in the presence of severe and persistent RFI.

Recent research efforts have increasingly explored alternative sensing and estimation technologies for formation flight that would overcome the limitations of both conventional SKE and of GPS-based relative positioning. The wide array of technologies that have been considered for aircraft (and also spacecraft) formation-flight applications includes ultra-wideband ranging (UWB) [16]; line-of-site (LOS) angular measurements using monocular cameras, laser systems, or systems operating in other parts of the electromagnetic spectrum [17]-[20]; and even detection of vortices generated by the lead aircraft of the formation [21]. The most practical of these technologies rely on the use of LOS and ranging measurements. These signals can be incorporated into jam-resistant, low-probability of detection systems that address the limitations of both conventional SKE and GPS-based technologies.

Accordingly, this paper investigates the use of LOS and ranging measurements for relative positioning when measurements are communicated throughout a formation, such that the set of estimated states is typically over-determined. In this situation, a "snapshot" solution is possible, meaning that relative positions can be computed using measurements only from a single instant in time. By contrast, most prior state-estimation studies using LOS and ranging measurements attain observability only when fusing data from multiple time steps with a Kalman Filter. A second distinctive feature of the proposed relative-positioning algorithm is that it can incorporate pseudo-ranging measurements, which are time-of-flight measurements acquired for pairs of vehicles whose clocks are not precisely synchronized. For precise ranging in the absence of synchronized clocks, the unknown offset of each aircraft's clock, relative to the leader's clock, must be determined through state estimation.

The paper is organized as follows. The next section (Section III) provides a detailed description of the proposed collaborative positioning algorithm and compares it to a more conventional SKE algorithm, in which aircraft do not communicate their measurements to other members of the formation. Section IV introduces a reference formation geometry which will be used in simulations to evaluate algorithm performance. Section V uses simulations to compare collaborative and conventional SKE algorithms for relative position estimation and assess the benefits and limitations of each. A brief summary concludes the paper.

III. Independent and Collaborative Aircraft Positioning

This section discusses two algorithms for estimating relative positions of aircraft in a formation: one algorithm representative of conventional SKE and a new collaborative algorithm that exploits an over-determined set of shared measurements.

The conventional algorithm estimates relative position by using slant range, altimeter, and bearing data directly to compute the position vector between a pair of aircraft. This approach uses only data collected by the ownship and is hence referred to as Independent Aircraft Positioning (IAP). As illustrated in Fig. 1(a), a particular aircraft estimates the relative positions of all other aircraft using only the data it collects, without referencing any of the range or bearing data collected by other aircraft in the formation.

By comparison to the conventional algorithm, the collaborative algorithm leverages shared data communicated among teamed aircraft. As such, this algorithm is referred to as Collaborative Multi-Aircraft Positioning (CMAP). The CMAP concept is illustrated in Fig. 1(b), which indicates ranging and bearing data being measured and shared among all aircraft collaborators. In the case shown, each of six unique aircraft pairs generates two ranging measurements, one in each direction, for a total of twelve ranging measurements (and, similarly, a total of twelve bearing measurements). Each aircraft uses all available measurement data (all twelve ranges and all twelve bearings in the case illustrated) to estimate its own position relative to all collaborating aircraft. Although it would conceptually be possible to compute this solution at a single, centralized processor, it is envisioned, instead, that each individual aircraft would compute the solution in parallel, effectively de-centralizing processing to enhance robustness and minimize communication delays.

The mathematical descriptions of the IAP and CMAP algorithms in this section share several common assumptions.

- Equipment is available to measure slant range between aircraft pairs based on an estimated time-of-flight of the transmitted signal.
- Equipment is available to measure a horizontal bearing angle between aircraft (i.e. azimuth) but not the vertical angle (i.e. elevation).
- Navigation-grade gyros and barometric altimeters are available on each aircraft.

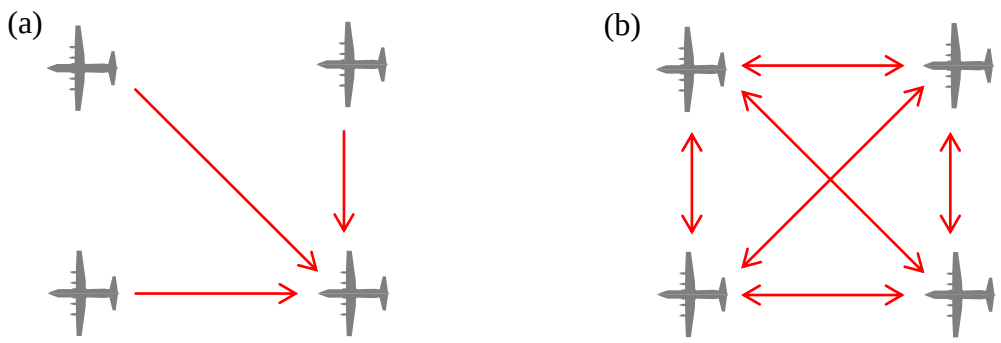

Fig. 1. Comparison of two algorithms. (a) IAP solves for relative positions of each aircraft pair independently, whereas (b) CMAP pools measurements and performs a coupled solution.

A. Independent Aircraft Positioning (IAP)

IAP assumes no data communication among aircraft. The estimated vector $\hat{\mathbf{x}}_{ij}$ that describes the relative position of a transmitting aircraft i to a particular receiving aircraft j is computed in North, East, and down coordinates ($\hat{n}_{ij}$, $\hat{e}_{ij}$, $\hat{d}_{ij}$) as follows. Here the hat notation indicates estimated terms; terms without hats are obtained from direct measurements.

$$\hat{\mathbf{x}}_{ij} = \begin{bmatrix} \hat{n}_{ij} \\ \hat{e}_{ij} \\ \hat{d}_{ij} \end{bmatrix} = \begin{bmatrix} \sqrt{r_{ij}^2 - \hat{h}_{ij}^2}\cos(\alpha_{ij}) \\ \sqrt{r_{ij}^2 - \hat{h}_{ij}^2}\sin(\alpha_{ij}) \\ -\hat{h}_{ij} \end{bmatrix} \tag{1}$$

The estimated position vector is a function of the slant range measurement r_{ij}, the bearing angle measurement α_{ij}, and the relative height estimate $\hat{h}_{ij}$, which is in turn based on the receiving aircraft's altimeter measurement a_j.

$$\hat{h}_{ij} = {}^{ref}a_i - a_j \tag{2}$$

In the absence of data communication, it is assumed that the receiving aircraft does not know the altitude of the transmitting aircraft; hence, the relative height estimate $\hat{h}_{ij}$ compares the receiving aircraft's altimeter to a pre-agreed reference value ${}^{ref}a_i$, which is the target altitude to be maintained by the transmitting aircraft. Given typical formation geometry, horizontal distances are much larger than vertical distances within the formation, so moderate

errors (tens of meters) in the altitude of the transmitting aircraft away from the nominal reference introduce little error in estimating $\hat{\mathbf{x}}_{ij}$.

It should be noted that (1) assumes all bearing angles are reported relative to North. In other words, raw LOS angle of arrival measurements are assumed to be projected into the horizontal plane and converted from a body-fixed angle ${}^{b}\alpha_{ij}$ (where the *b* superscript indicates body-fixed coordinates) into an inertially fixed bearing angle α_{ij} , defined relative to North. This conversion requires knowledge of the receiving aircraft's yaw heading ψ_j, which is assumed to be obtained from an inertial navigation system.

$$\alpha_{ij} = {}^{b}\alpha_{ij} + \psi_j \tag{3}$$

It is further implicitly assumed (in conventional IAP, but not in CMAP) that all aircraft are equipped with synchronized atomic clocks, such that the range measurement r_{ij} can be computed in an unbiased fashion from the time-of-flight. An agreed upon transmission time is also assumed (e.g. transmission occurs at the top of each second), such that the transmitter aircraft need not time tag its broadcast.

In practice, station keeping is possible by estimating a position relative to only one other aircraft, which is designated as the leader of the formation. Without loss of generality, the leader aircraft will be identified by an index *i* equal to 1. To perform station keeping relative to the leader, each follower aircraft *j* need only evaluate equation (1) once, to estimate the position vector $\mathbf{x}_{1j}$.

Although the IPA relative position equations are nonlinear, small errors in the estimated position vector can be modeled using a linearized analysis. Errors in the estimated position vector $\boldsymbol{\varepsilon}_{\mathbf{x},ij}$ can be related to the sensor error vector $\boldsymbol{\varepsilon}_{\mathbf{y},ij}$ by the following equation.

$$\boldsymbol{\varepsilon}_{\mathbf{x},ij} = \mathbf{H}_{ij}^{-1}\boldsymbol{\varepsilon}_{\mathbf{y},ij} \tag{4}$$

Here $\boldsymbol{\varepsilon}_{\mathbf{y},ij}$ is the sensor error for the following sensor measurement vector $\mathbf{y}$,

$$\mathbf{y}_{ij} = \begin{bmatrix} r_{ij} & \alpha_{ij} & a_j \end{bmatrix}^T, \tag{5}$$

and $\mathbf{H}_{ij}^{-1}$ is the derivative matrix (i.e. Jacobian) of the relative position estimation equation (1) with respect to $\mathbf{y}$.

$$\mathbf{H}_{ij}^{-1} = \begin{bmatrix} \dfrac{r_{ij}\cos(\alpha_{ij})}{\sqrt{r_{ij}^2 - \hat{h}_{ij}^2}} & -\sqrt{r_{ij}^2 - \hat{h}_{ij}^2}\sin(\alpha_{ij}) & \dfrac{\hat{h}_{ij}\cos(\alpha_{ij})}{\sqrt{r_{ij}^2 - \hat{h}_{ij}^2}} \\ \dfrac{r_{ij}\sin(\alpha_{ij})}{\sqrt{r_{ij}^2 - \hat{h}_{ij}^2}} & \sqrt{r_{ij}^2 - \hat{h}_{ij}^2}\cos(\alpha_{ij}) & \dfrac{\hat{h}_{ij}\sin(\alpha_{ij})}{\sqrt{r_{ij}^2 - \hat{h}_{ij}^2}} \\ 0 & 0 & -1 \end{bmatrix} \tag{6}$$

The inverse notation is used because **H** typically represents a sensor model, which maps perturbations in the states to perturbations in the measured sensor data [22].

Using these equations and assuming unbiased Gaussian statistics, an error model for the relative-position estimate can be fully specified using a covariance matrix. For small measurement errors, the state-error covariance matrix $\mathbf{P}_{ij}$ is related to the sensor covariance matrix $\mathbf{R}_{ij}$ by the following linearized model.

$$\mathbf{P}_{ij} = E\left[\boldsymbol{\varepsilon}_{\mathbf{x},ij}\boldsymbol{\varepsilon}_{\mathbf{x},ij}^T\right] = \mathbf{H}_{ij}^{-1}\mathbf{R}_{ij}\mathbf{H}_{ij}^{-T} \tag{7}$$

In this paper, sensor errors are modeled as independent, Gaussian and unbiased. Accordingly, the sensor covariance matrix is given by the following equation, where σ_r is the standard deviation of the ranging error, σ_α is the standard deviation of the bearing error, and σ_a is the standard deviation of the altimeter.

$$\mathbf{R}_{ij} = E\left[\boldsymbol{\varepsilon}_{\mathbf{y},ij}\boldsymbol{\varepsilon}_{\mathbf{y},ij}^T\right] = \begin{bmatrix} \sigma_r^2 & 0 & 0 \\ 0 & \sigma_\alpha^2 & 0 \\ 0 & 0 & \sigma_a^2 \end{bmatrix} \tag{8}$$

It is assumed that the error of the inertially estimated aircraft yaw angle ψ_j is held small relative to the instantaneous errors of the body-frame angle of arrival ${}^b\alpha_{ij}$. Thus, gyro errors are not explicitly considered in this analysis.

In subsequent sections, the state-error covariance model (7) will be used to estimate the performance of the IAP algorithm and to compare it with CMAP.

B. Collaborative Multi-Aircraft Positioning (CMAP)

This section introduces CMAP, an alternative formulation for estimating aircraft relative positions. CMAP collaboratively shares measurements throughout the formation in order to reduce sensitivity to bearing measurement

error. To take advantage of measurement sharing, the relative positions of all aircraft are estimated simultaneously. The formation state vector $\mathbf{x}_f$ includes estimates for the positions of not just one aircraft relative to another, as in (1), but for all aircraft relative to a leader.

$$\mathbf{x} = \begin{bmatrix} n_{12} & e_{12} & d_{12} & b_{12} & \cdots & n_{1N} & e_{1N} & d_{1N} & b_{1N} \end{bmatrix}^T \tag{9}$$

Here the leader is designated as aircraft 1, and the followers are designated with indices from 2 through *N*. The vector $\mathbf{x}_f$ comprises a set of four estimated states for each follower. Three of these are relative positions in north, east and down coordinates (n_{ij}, e_{ij}, and d_{ij}). The fourth is an inter-aircraft clock bias b_{ij}, a state which was not previously modeled in the discussion of the IAP algorithm. Introducing the clock bias for each aircraft as a state effectively relaxes an assumption made previously, allowing for the use of lower quality clocks (e.g. quartz oscillators) or for continuous synchronization of high quality clocks (e.g. atomic clocks), which may be necessary during longer missions. To ensure a well-conditioned numerical solution, the relative clock error is reported in units of length (e.g. $b_{ij} = c\Delta_{ij}$, where the time offset Δ_{ij} is scaled by the speed of light *c*).

Observation of clock drift is possible using two-way ranging. Using the variable ρ_{ij} to denote the pseudorange (the clock-corrupted range measurement), it is possible to decompose the pseudorange in terms of the true range r_{ij} and the relative clock error b_{ij}.

$$\rho_{ij} = r_{ij} - b_{ij} \tag{10}$$

The true range is the same for *i* relative to *j* and *vice versa* ($r_{ij} = r_{ji}$). However, the clock error changes sign for each case ($b_{ij} = -b_{ji}$). Hence, the measured *pseudorange* is longer than the true range (by the clock drift) in one direction and shorter in the other.

$$\rho_{ij} = \rho_{ji} - 2b_{ij} \tag{11}$$

In order to estimate the clock bias term b_{ij}, bi-directional measurements are assumed in comparison to the single-directional measurements used for IAP. In other words, slant range and bearing measurements are acquired from aircraft *i* to *j* and also from *j* to *i* (see Fig. 1). Moreover, measurements are assumed to be acquired between every aircraft pair. Assuming that *N* aircraft in a formation share measurements, then each of these aircraft produces a

slant range measurement to N-1 other aircraft, for a total of $N(N\text{-}1)$ slant range measurements. Another $N(N\text{-}1)$ bearing measurements, one for each ordered pair of aircraft, and an additional N-1 differential altimeter measurements, one for each follower, are also used in the estimation process. Hence, the total number of measurements is $(2N+1)(N\text{-}1)$. A vector $\mathbf{y}_f$ is defined as the formation-level sensor vector that contains all $(2N+1)(N\text{-}1)$ measurements used to obtain the CMAP solution.

$$\mathbf{y}_f = \begin{bmatrix} \rho_{12} & \alpha_{12} & \cdots & \rho_{N(N-1)} & \alpha_{N(N-1)} & h_{12} & \cdots & h_{1N} \end{bmatrix}^T \tag{12}$$

This formation-level sensor vector consists of two sub-blocks. In the first block, range and bearing measurements are listed in an alternating fashion for each ordered aircraft pair (i,j). In the second block, relative height measurements are listed for each follower aircraft relative to the leader. These relative height measurements are generated from a difference of two altimeter measurements, a_i and a_j.

$$h_{ij} = a_i - a_j \tag{13}$$

Note in CMAP, in contrast with IAP, it is assumed that altimeter measurements are communicated throughout the formation, hence relative positioning does not depend on an assumed reference height as in (2).

The CMAP algorithm must estimate the state vector (9) from the measurement vector (12) using an appropriate measurement model. In the case of CMAP, the number of measurements is larger than the number of states, except when the number of collaborating aircraft N is 2. (When the formation consists of only two aircraft, then the number of measurements is exactly sufficient to compute a relative position.) Hence, the computed estimate should take advantage of redundancy to minimize the error of the state estimate $\hat{\mathbf{x}}_f$. To minimize state-estimation error, CMAP relies on an iterative (Newton-Raphson) least-squares formulation, as is often used in solving nonlinear navigation problems with redundant measurements, such as GPS positioning [23]. To obtain this solution, an initial state estimate is assumed; then the state estimate is iteratively improved to convergence by solving a linearized correction equation at each step. In CMAP, the linearized correction equation has the following form.

$$\mathbf{B}\delta\hat{\mathbf{x}}_f = \mathbf{A}\delta\mathbf{y}_f \tag{14}$$

The matrices **A** and **B** will be obtained by linearizing measurement equations very similar to (1), as described below. At each iteration, the improved state estimate is obtained by updating the old state estimate $\hat{\mathbf{x}}_f$ as follows.

$$\hat{\mathbf{x}}_f \Rightarrow \hat{\mathbf{x}}_f + \delta\hat{\mathbf{x}}_f \tag{15}$$

Here the perturbed state estimate is computed by obtaining a weighted least-squares solution [22] to the over-constrained equation set (14).

$$\delta\mathbf{x}_f = \left(\mathbf{B}^T\mathbf{W}\mathbf{B}\right)^{-1}\mathbf{B}^T\mathbf{W}\mathbf{A}\delta\mathbf{y}_f \tag{16}$$

The particular weighting matrix used in this application is a function of the **A** matrix and the measurement covariance matrix $\mathbf{R}_f$.

$$\mathbf{W} = \left(\mathbf{A}\mathbf{R}_f\mathbf{A}^T\right)^{-1} \tag{17}$$

This form for **W** simplifies state-error covariance analysis, as will be described later in the section.

The matrices **A** and **B** are obtained by linearizing equations that are essentially equivalent to (1), except that the relative height measurement h_{ij} of (13) is substituted for the estimated $\hat{h}_{ij}$ of (2), and that an estimated range $\hat{r}_{ij}$ is substituted for the true range r_{ij}. The estimated range accounts for the unknown clock offset $\hat{b}_{ij}$ as follows.

$$\hat{r}_{ij} = \rho_{ij} + \hat{b}_{ij} \tag{18}$$

Linearizing this weakly modified form of vector equation (1) gives the following three scalar equations.

$$\delta\hat{n}_{ij} - \left(\frac{\hat{r}_{ij}}{\hat{p}_{ij}}\cos\alpha_{ij}\right)\delta\hat{b}_{ij} = \left(\frac{\hat{r}_{ij}}{\hat{p}_{ij}}\cos\alpha_{ij}\right)\delta\rho_{ij} - \left(\hat{p}_{ij}\sin\alpha_{ij}\right)\delta\alpha_{ij} + \left(\frac{h_{ij}}{\hat{p}_{ij}}\cos\alpha_{ij}\right)\delta h_{ij} \tag{19}$$

$$\delta\hat{e}_{ij} - \left(\frac{\hat{r}_{ij}}{\hat{p}_{ij}}\sin\alpha_{ij}\right)\delta\hat{b}_{ij} = \left(\frac{\hat{r}_{ij}}{\hat{p}_{ij}}\sin\alpha_{ij}\right)\delta\rho_{ij} + \left(\hat{p}_{ij}\cos\alpha_{ij}\right)\delta\alpha_{ij} + \left(\frac{h_{ij}}{\hat{p}_{ij}}\sin\alpha_{ij}\right)\delta h_{ij} \tag{20}$$

$$\delta d_{ij} = -\delta h_{ij} \tag{21}$$

In these equations, δ denotes a small perturbation. The variable $\hat{p}_{ij}$ is introduced as shorthand to denote the planar range estimate:

$$\hat{p}_{ij} = \sqrt{\left(\rho_{ij} - \hat{b}_{ij}\right)^2 - h_{ij}^2} \ . \tag{22}$$

Equations (19)-(21) are not yet expressed entirely in terms of the components of the state and sensor vector given by (9) and (12). The problem is that the state vector expresses the position of each follower relative to the leader. To recover these states, the following substitutions are made.

$$\begin{aligned}
\delta\hat{n}_{ij} &= \delta\hat{n}_{1i} - \delta\hat{n}_{1j} \\
\delta\hat{e}_{ij} &= \delta\hat{e}_{1i} - \delta\hat{e}_{1j} \\
\delta\hat{d}_{ij} &= \delta\hat{d}_{1i} - \delta\hat{d}_{1j} \\
\delta\hat{b}_{ij} &= \delta\hat{b}_{1i} - \delta\hat{b}_{1j} \\
dh_{ij} &= \delta a_{1i} - \delta a_{1j}
\end{aligned} \tag{23}$$

Each of the first four variables is rewritten as the difference of two states in $\mathbf{x}_f$. The fifth variable is rewritten as the difference of two altimeter values in the sensor vector $\mathbf{y}_f$. In order to make (23) suitably general, the position and clock shifts for the first aircraft relative to itself are assumed to be zero:

$$\delta\hat{n}_{11} = \delta\hat{e}_{11} = \delta\hat{d}_{11} = \delta\hat{b}_{11} = \delta a_{11} = 0 . \tag{24}$$

The matrices **A** and **B** can now be generated from (19)-(21), substituting (23) and (24) where appropriate. The rows of **A** and **B** are assigned such that each generates an equation corresponding to one of the components of the sensor vector $\mathbf{y}_f$, as described by (12). Accordingly, the rows of **A** and **B** can be decomposed into two blocks. The first block, consisting of rows 1 through $2N(N\text{-}1)$, consists of alternating equations for each possible aircraft pairing (i,j); the two alternating equations for each of these aircraft pairings are generated from the linearized North and East equations, (19) and (20), respectively. The second block of rows, consisting of an additional N-1 equations, correspond to the heights of each aircraft relative to the lead; the equations for each row in the second block are generated by repeatedly evaluating the linearized downward-axis equation (21) for each follower aircraft.

It is worth noting that the linearization procedure described here is somewhat unconventional; other strategies might also be used to obtain a linearized model relating the vector of states $\mathbf{x}_f$ to the vector of sensor data $\mathbf{y}_f$. For instance, a more conventional linearization method would be to use a Taylor series expansion for the following nonlinear sensor model $\hat{\mathbf{y}}_f$.

$$\hat{\mathbf{y}}_f(\hat{\mathbf{x}}_f) = \begin{bmatrix} \sqrt{\hat{n}_{12}^2 + \hat{e}_{12}^2 + \hat{d}_{12}^2} + \hat{b}_{12} \\ \operatorname{atan2}\left(\hat{e}_{i12}, \hat{n}_{12}\right) \\ \vdots \\ \sqrt{\hat{n}_{N(N-1)}^2 + \hat{e}_{N(N-1)}^2 + \hat{d}_{N(N-1)}^2} + \hat{b}_{N(N-1)} \\ \operatorname{atan2}\left(\hat{e}_{N(N-1)}, \hat{n}_{N(N-1)}\right) \\ d_{12} \\ \vdots \\ d_{1N} \end{bmatrix} \tag{25}$$

This more conventional approach is not conducive to an iterative numerical solution, however, because the value of the `atan2` function (the form of the arctangent function defined over all four quadrants) is discontinuous at $\pm\frac{1}{2}\pi$ and because its slope goes to zero at these discontinuity points. As a consequence the Newton-Raphson equations do not guarantee that it is possible to push an initial guess from one side of the discontinuity (e.g. from $\frac{1}{2}\pi - \varepsilon$) to the other (e.g. to $\frac{1}{2}\pi + \varepsilon$). By comparison, equations (19)-(21) use sine and cosine functions, which are continuously defined over all four quadrants, and which are numerically well behaved in solving the weighted least-squares problem given by (16).

The CMAP solution has been fully defined with one exception. In order to solve (15) and (16) iteratively to estimate the system states, it is necessary to compute the sensor model discrepancy $\delta\mathbf{y}_f$ at each iteration. This discrepancy is the difference between the raw sensor measurements and the sensor model given by (25).

$$\delta\mathbf{y}_f = \mathbf{y}_f - \hat{\mathbf{y}}_f(\hat{\mathbf{x}}_f) \tag{26}$$

Although the system of equation solved by (15), (16), and (26) is nonlinear, it is possible to use a linear error analysis to approximate the state-estimation error covariance matrix when measurement errors are small. Assuming the measurement error vector $\boldsymbol{\varepsilon}_{\mathbf{y}_f}$ is additive, the state-estimation covariance matrix is $\mathbf{P}_f$.

$$\mathbf{P}_f = E\left[\boldsymbol{\varepsilon}_x \boldsymbol{\varepsilon}_x^T\right] = \left(\mathbf{B}^T\mathbf{W}\mathbf{B}\right)^{-1}\mathbf{B}^T\mathbf{W}\mathbf{A}\mathbf{R}_f\mathbf{A}^T\mathbf{W}^T\mathbf{B}\left(\mathbf{B}^T\mathbf{W}\mathbf{B}\right)^{-1} \tag{27}$$

Here $\mathbf{R}_f$ is the sensor error covariance matrix $\left(\mathbf{R}_f = E\left[\boldsymbol{\varepsilon}_{\mathbf{y}_f}\boldsymbol{\varepsilon}_{\mathbf{y}_f}^T\right]\right)$. Substituting the expression for the weighting matrix **W**, as given by (17), into the state covariance equation above results in the following simplification.

$$\mathbf{P}_f = \left(\mathbf{B}^T\left(\mathbf{A}\mathbf{R}_f\mathbf{A}^T\right)^{-1}\mathbf{B}\right)^{-1} \tag{28}$$

The basic CMAP algorithm has the potential for significant reduction of state-estimation errors as compared to IAP. Error mitigation is possible in large part because of the availability of redundant measurements. Least-squares processing of redundant measurements effectively averages and shrinks measurement error. The inclusion of the weighting matrix **W** de-emphasizes less accurate measurements and further mitigates uncertainty. This capability to de-emphasize inaccurate measurements is of particular importance when bearing measurement errors are large. In fact, if the bearing measurement errors are sufficiently de-weighted by **W**, CMAP performs what is essentially a range-only solution for all-but-one degree of freedom in the estimated state vector, namely, the formation rotation angle. This limiting case is discussed in more detail in the following section.

C. CMAP Post-Processing

For applications involving especially large bearing-measurement errors, the error mitigation properties of the basic CMAP algorithm may not be sufficient to meet relative-positioning accuracy requirements. Consequently, this section discusses additional post-processing that significantly reduces the sensitivity of CMAP to bearing measurement errors.

In order to understand how post-processing can reduce the impact of large bearing errors, it is useful to consider the limiting case when bearing measurement error tends toward infinity. This is essentially equivalent to the case in which bearing measurements are entirely absent. In the absence of bearing measurements, it is still possible to estimate the shape of a formation, in the sense that the formation "shape" is described as a mesh of triangles with one aircraft at each vertex. The structure of this triangular mesh is fully determined by the length of the sides of each triangle; hence, ranging data is sufficient to infer this structure.

The rigid-body rotation of the mesh (e.g. the rotation angle of the entire formation relative to North) cannot be determined without bearing data, however. Fig. 2 illustrates this limitation. The figure shows the same set of aircraft in two configurations. In both configurations, the distances between particular aircraft pairs are the same; hence the ranging measurements are the same in each case. The two configurations are distinct in that they are globally rotated, as described by the formation-rotation angle α_f. This global rotation cannot be inferred from ranging data alone. As a consequence, bearing measurement data – even highly uncertain bearing measurement data – is essential to CMAP processing.

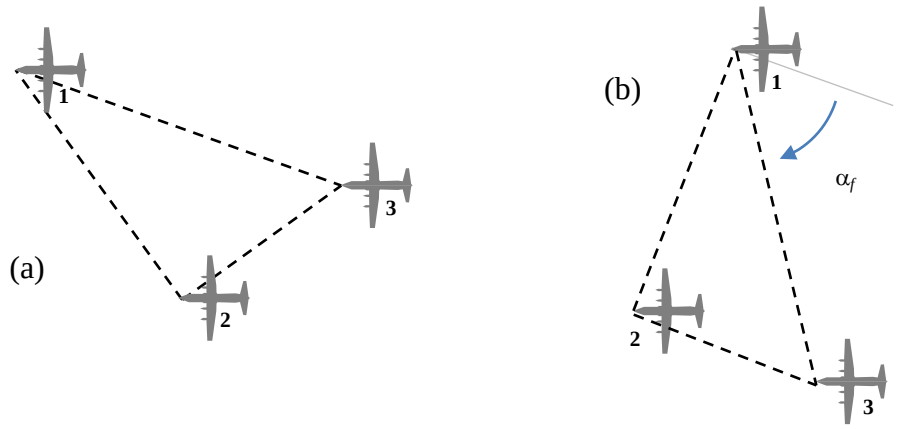

Fig. 2. Rotational ambiguity for range-only relative-position estimation. It is possible to rotate the nominal configuration (a) through any angle α_f without changing the range between aircraft pairs, as is exemplified by configuration (b).

Although CMAP depends on bearing data, post-processing can be introduced to reduce their impact on CMAP accuracy. Specifically, post-processing can be introduced to low-pass filter the formation-rotation angle α_f. Implicitly, it is assumed that the formation rotation angle changes very slowly, as it is unlikely that random perturbations cause large coordinated drifts that swing the entire formation out of alignment with its nominal orientation. (In the case of a formation maneuver, it is assumed that the nominal orientation angle is a time-varying quantity, one which is communicated among all collaborators.) Moreover, because filtering can introduce a control system lag that limits controller performance, and because it is desirable that formation-flight control laws tightly maintain inter-aircraft distances at all times, it assumed that filtering should be applied only to smooth the global rotation angle and not to smooth any other degree-of-freedom of the CMAP state estimate.

The following methodology is proposed as a mechanism to smooth the formation-rotation angle without introducing a lag into any other state estimated by CMAP. The methodology consists of three post-processing steps, as illustrated in Fig. 3. First, the method computes an instantaneous rotation estimate $\hat{\alpha}_f$ relative to a control reference. Second, the instantaneous estimate is filtered to produce the smoothed estimate $\bar{\alpha}_f$. Finally, the estimated states of $\hat{\mathbf{x}}_f$ are de-rotated so that they align with the smoothed rotation angle $\bar{\alpha}_f$.

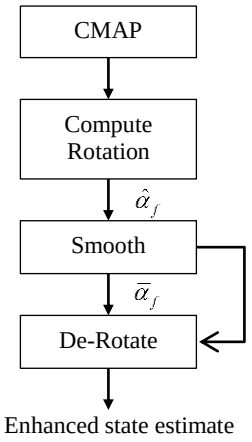

Fig. 3. Block diagram for CMAP post-processing

In the first post-processing step (*Compute Rotation* block in Fig. 3), the estimated states of the $\hat{\mathbf{x}}_f$ vector are compared to a set of reference states, which represent targets for closed-loop control. The best estimate of the instantaneous formation-rotation angle can be obtained by minimizing a cost function. This cost function compares the North and East reference coordinates ($^{ref}n_{1j}$ and $^{ref}e_{1j}$) for each follower *j* to the corresponding estimated coordinates ($\hat{n}_{1j}$ and $\hat{e}_{1j}$) for the same aircraft, given an arbitrary formation-rotation angle α_f. The best estimate of the formation-rotation angle is that which best aligns the reference and estimated coordinates, minimizing the cost function *J*.

$$
\begin{aligned}
J &= \sum_{j=2}^{N} \mathrm{r}_j^T \, \mathrm{r}_j \\
\mathrm{r}_j &= \mathbf{\Phi}\left(-\alpha_f\right)\begin{bmatrix} \hat{n}_{1j} \\ \hat{e}_{1j} \end{bmatrix} - \begin{bmatrix} {}^{ref}n_{1j} \\ {}^{ref}e_{1j} \end{bmatrix}
\end{aligned}
\tag{29}
$$

Here, the planar rotation matrix $\mathbf{\Phi}$ rotates the estimated states opposite the angle α_f in order to align them with the reference states . To find the best estimate of α_f, it is useful to consider the slope of the cost function *J*. Where the cost function reaches its minimum value, the slope of the cost function is zero. Thus, the best estimate of α_f can be obtained by solving the following nonlinear equation.

$$\frac{dJ}{d\alpha_f} = \sum_{j=2}^{N} \left(\gamma_j \sin\alpha_f + \chi_j \cos\alpha_f \right) = 0 \tag{30}$$

Here the coefficients γ_j and χ_j for each aircraft are formed from a dot-product and from a cross-product as follows.

$$\begin{aligned} \gamma_j &= {}^{ref}n_{1j}\,\hat{n}_{1j} + {}^{ref}e_{1j}\,\hat{e}_{1j} \\ \chi_j &= {}^{ref}e_{1j}\,\hat{n}_{1j} - {}^{ref}n_{1j}\,\hat{e}_{1j} \end{aligned} \tag{31}$$

Nonlinear equation (30) can be quickly solved by using Newton-Raphson iterations in which the estimate of the formation-rotation angle $\hat{\alpha}_f$ is iteratively corrected by a small perturbation $\delta\hat{\alpha}_f$.

$$\hat{\alpha}_f \Rightarrow \hat{\alpha}_f + \delta\hat{\alpha}_f \tag{32}$$

At each iteration, the perturbation $\delta\hat{\alpha}_f$ is computed by evaluating the following equation, derived from a Taylor Series Expansion of (30).

$$\delta\alpha_f = \frac{-\sum_{j=2}^{N} \left(\gamma_j \sin\hat{\alpha}_f + \chi_j \cos\hat{\alpha}_f \right)}{\sum_{j=2}^{N} \left(\gamma_j \cos\hat{\alpha}_f - \chi_j \sin\hat{\alpha}_f \right)} \tag{33}$$

The resulting estimation of $\hat{\alpha}_f$ converges quickly, typically within 2-3 iterations given an assumed initial value of zero.

An important observation is that the slope of *J*, given by (30), reaches zero not only at the cost function minimum, but also at its maximum. The iterative Newton-Rhapson procedure may thus, at least in theory, produce either the best or worst possible estimate of the true α_f. The best and worst angle estimates are out of phase by 180°, at opposite extents of a circle. Thus it is trivial to verify the minimum by evaluating the cost function *J* for two

angles $\hat{\alpha}_f$ and $\hat{\alpha}_f + \pi$. Whichever of these two extrema has the lower cost should be used as the best estimate of the formation-rotation angle.

The second post-processing step (*Smooth* block in Fig. 3) applies a low-pass filter to the estimated formation rotation angle. A variety of filtering options might be considered; for instance, a Kalman filter might be used to predict coordinated changes in the orientation of the formation during a planned maneuver. For purposes of illustration, this paper considers only straight-line flight. For the case of straight-line flight, it is sufficient to compute the smoothed formation-rotation angle $\bar{\alpha}_f$ using a simple first-order linear filter, which is applied at each time step *k*.

$$\bar{\alpha}_f(k) = \left(1 - \frac{T}{\tau}\right)\bar{\alpha}_f(k-1) + \frac{T}{\tau}\hat{\alpha}_f(k) \tag{34}$$

The constant parameters T and τ are the sample interval and the time constant, respectively. The low-pass filter reduces the error of the smoothed angle $\bar{\alpha}_f$ relative to the instantaneous estimate $\hat{\alpha}_f$ by an amount that depends on the time-correlation of the error of the instantaneous estimate. If, for instance, bearing-measurement errors are not time-correlated (i.e. if the errors are white), then the smoothing process reduces the standard deviation of the smoothed angle by a factor of approximately $\sqrt{T/\tau}$.

The final post-processing step (*De-Rotate* block in Fig. 3) applies the smoothed formation-rotation angle to correct the state estimate vector $\hat{\mathbf{x}}_f$. To compute the corrected North and East estimates ($^c\hat{n}_{1j}$ and $^c\hat{e}_{1j}$) for each aircraft *j*, the following equation is used.

$$\begin{bmatrix} {}^c\hat{n}_{1j} \\ {}^c\hat{e}_{1j} \end{bmatrix} = \mathbf{\Phi}\left(-\hat{\alpha}_f + \bar{\alpha}_f\right)\begin{bmatrix} \hat{n}_{1j} \\ \hat{e}_{1j} \end{bmatrix} \tag{35}$$

This equation resets the state estimates such that the formation is oriented at the smoothed angle $\bar{\alpha}_f$. To do this, the rotation matrix $\mathbf{\Phi}$ effectively removes (subtracts) the noisy instantaneous rotation angle $\hat{\alpha}_f$. Then the rotation matrix effectively inserts (adds) the improved estimate of the formation-rotation angle $\bar{\alpha}_f$, rotating the formation

back to the desired orientation. The final result is that the shape of the formation is estimated instantaneously, with no lag, while the global formation-rotation angle is low-pass filtered, to mitigate bearing measurement noise.

IV. Reference Formation

The performance of the IAP and CMAP methods described in the previous section is somewhat dependent on the geometry of the aircraft formation. Hence, a reference formation must be identified in order to compare the two algorithms. The reference formation is chosen to be functionally somewhat similar (but not identical) to formations commonly flown by military cargo aircraft.

For the purpose of this paper, the reference formation is defined to consist of multiple three-aircraft groupings called *elements*. A formation of arbitrary length can be created by stringing elements one after another in an extended column (see Fig. 4). The particular element shape chosen for this paper is an inverted-V formation [4] with lateral (cross-track) spacing of 200 m and longitudinal (in-track) spacing of 1500 m between aircraft. A wider in-track gap of 6000 m is assumed between successive elements.

Without loss of generality, simulations always assume that the formation is traveling due West. Hence relative positioning errors in the North direction can also be described as cross-track deviations. Similarly, errors in the East direction are described as in-track deviations. Aircraft in the formation are indexed counting from the lead aircraft, which is designated AC1, and incrementing for each follower.

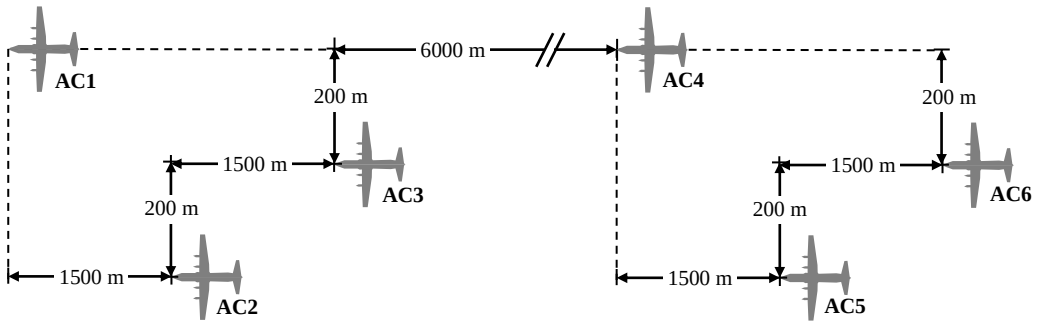

Fig. 4. Reference formation with two elements, each consisting of three aircraft

V. Simulations

This section describes simulations used to compare the performance of the IAP and CMAP algorithms. In particular, simulations are used to evaluate the performance of algorithms for varying levels of bearing measurement error, since bearing errors have a pronounced effect on relative positioning accuracy when spacing between aircraft is large (e.g. several kilometers, as is the case for the reference formation). To assess the impact of these variations, in-track and cross-track positioning errors are reported for each algorithm as a function of bearing measurement error. More specifically, simulations are used to characterize the standard deviations for relative positioning in the in-track and cross-track directions for each of the first three follower aircraft (AC2-AC4).

A. Error Models

The primary goal of simulation is to characterize how the IAP and CMAP algorithms perform as bearing-measurement accuracy degrades. As such, algorithms are tested for a range of bearing accuracy values, starting at a minimum standard deviation σ_α of 0.1° and proceeding up to a maximum of 30°. For the purposes of simulation, bearing measurement errors are assumed independent and Gaussian.

Slant range and altimeter accuracy are fixed for all simulations. Range and altimeter errors are also assumed Gaussian and independent, with a standard deviation of σ_r (equal to 2 m) for each slant ranging measurement and of σ_a (equal to 10 m) for each altimeter. It must be noted that the estimation algorithms do not use altimeter data directly. Rather, they depend on a height difference, as defined by (2) for IAP and (13) for CMAP. Assuming independent Gaussian errors, the variance of the height differences is twice that of the raw altimeter measurements; moreover, for the CMAP algorithm, height differences for various followers are correlated, since all differences are computed relative to the lead aircraft. To account for this correlation, a height difference covariance matrix $\mathbf{R}_h$ is introduced. The elements of this matrix have the following form.

$$\mathbf{R}_{h,ij} = E\left[\left(a_1 - a_i\right)\left(a_1 - a_j\right)\right] = \begin{cases} 2\sigma_a^2 & i = j \\ \sigma_a^2 & i \neq j \end{cases} \tag{36}$$

For the CMAP algorithm, inaccurate clocks are permitted, so ranging measurements are assumed to suffer from clock jitter. As such, random clock offsets (b_{ij}) are added to each ranging error to convert it to a pseudorange error.

For the purposes of this work, each pseudorange error $\varepsilon_{\rho,ij}$ is equal to a ranging error $\varepsilon_{r,ij}$ shifted by the bias between the transmitting aircraft clock error $\varepsilon_{b,i}$ and that of the receiving aircraft $\varepsilon_{b,j}$.

$$\varepsilon_{\rho,ij} = \varepsilon_{r,ij} + \underbrace{\left(\varepsilon_{b,j} - \varepsilon_{b,i}\right)}_{b_{ij}} \tag{37}$$

In simulating pseudoranges, ranging errors $\varepsilon_{r,ij}$ are assumed to be zero-mean Gaussian with a standard deviation of σ_r (as described above). The clock jitter error for each aircraft $\varepsilon_{b,i}$ is assumed to be zero-mean Gaussian with a standard deviation of σ_b (equal to 100 m). Here the clock error has units of length (rather than time), due to scaling by the speed of light to improve the condition number of the matrices used in computing the CMAP solution.

Although clock errors are included in Monte Carlo simulations of CMAP, these errors are considered as state errors (not as sensor errors) because the clock biases b_{ij} are directly estimated as states. Hence the sensor error covariance matrix does not depend on σ_b. Given the structure of the CMAP sensor vector $\mathbf{y}_f$, defined by (12), the corresponding sensor error covariance matrix $\mathbf{R}_f$ for CMAP has the following form.

$$\mathbf{R}_{f,ij} = \begin{cases} \sigma_r^2 & i = j \in 1,3,...,2N(N-1)-1 \\ \sigma_\alpha^2 & i = j \in 2,4,...,2N(N-1) \\ \mathbf{R}_{h,ij} & i,j > 2N(N-1) \\ 0 & \text{otherwise} \end{cases} \tag{38}$$

For N collaborating aircraft, the first $2N(N\text{-}1)$ diagonal elements are alternating variances for ranging and bearing measurements. These variances are assumed to have the same magnitudes for all aircraft pairs. The lower-right-corner of $\mathbf{R}_f$ is the sub-matrix $\mathbf{R}_h$, which is square with dimension N-1. All remaining elements of $\mathbf{R}_f$ are zero.

For the purposes of comparing the algorithms, it is assumed that the actual formation rotation angle α_f is always zero. Thus, any deviation of the estimated formation-rotation angle $\hat{\alpha}_f$ away from zero is clearly an error.

B. Simulation Methods

Simulations are used to evaluate the performance of the IAP algorithm, the baseline CMAP algorithm, and the CMAP algorithm augmented with post-processing. All three algorithms were tested for seven distinct levels of

bearing error (σ_α equal to 0.1°, 1°, 2.5°, 5°, 10°, 20°, 30°). In all, considering the three algorithms and seven levels of bearing error, twenty-one different scenarios were considered. One thousand independent Monte Carlo trials were run for each of these twenty-one scenarios. In each case, relative-position errors were quantified by computing standard deviations for the in-track and cross-track positions of each of the first three followers in the formation.

As a means to verify Monte Carlo (statistical) calculations, in-track and cross-track standard deviations were also computed using linearized (probabilistic) analysis. The linearized analysis evaluates the theoretical covariance matrices for IAP and CMAP using equations (7) and (28) respectively. Computing position estimation errors using two distinct approaches – namely, Monte Carlo simulations and linearized analysis – enables a cross-comparison to verify results. The two methods are expected to agree, especially when the assumptions of the linearized analysis are most appropriate (e.g. typically when measurement errors are smallest).

For the CMAP method with post-processing, a modification to the linearized analysis of (28) is required to account for the nonlinear de-rotation procedure. In order to obtain an appropriate correction, it is hypothesized that the baseline CMAP procedure depends only on ranging (and altimetry) data, and that the subsequent rotation angle estimation procedure depends only on bearing measurement data. In other words, it is hypothesized that post-processing effectively decouples the roles of ranging and bearing measurements in CMAP. By extension, smoothing performed in the post-processing procedure essentially reduces the magnitude of the bearing measurement errors, and as such the linearized state-error covariance matrix $\mathbf{P}_f$ should be computed using a modified sensor covariance matrix ${}^{sm}\mathbf{R}_f$. In the modified sensor covariance matrix, the variance of the raw bearing measurement error should be replaced by that of the smoothed bearing measurement error. For instance, in the case of white noise and the low pass filter of (34), the modified sensor covariance matrix is the following.

$$ {}^{sm}\mathbf{R}_{f,ij} = \begin{cases} \dfrac{T}{\tau}\sigma_\alpha^2 & i = j \in 2,4,...,2N(N-1) \\ \mathbf{R}_{f,ij} & \text{otherwise} \end{cases} \tag{39} $$

The resulting model for the state-error covariance matrix is thus:

$$ \mathbf{P}_f = \left(\mathbf{B}^T\mathbf{W}\mathbf{B}\right)^{-1}\mathbf{B}^T\mathbf{W}\mathbf{A}\,{}^{sm}\mathbf{R}_f\,\mathbf{A}^T\mathbf{W}^T\mathbf{B}\left(\mathbf{B}^T\mathbf{W}\mathbf{B}\right)^{-1}. \tag{40} $$

Note, in order to ensure that the basic CMAP procedure appropriately emphasizes ranging measurements over bearing measurements, it is critical that the weighting matrix **W** be computed in the conventional manner, by (17), which is based on the original $\mathbf{R}_f$ matrix. Using the original $\mathbf{R}_f$ matrix to computing the weighting reflects the fact that the weighting is based on errors prior to smoothing and not those post-smoothing (as modeled by ${}^{sm}\mathbf{R}_f$).

In order to evaluate the smoothed sensor covariance matrix of (39), some assumptions must be made regarding the nature of the low-pass filter. For the purposes of this paper, we assume White, Gaussian noise is present on samples acquired at 2 Hz (T = 0.5 sec) and subsequently smoothed with a time constant τ of 50 sec. The result is an order of magnitude suppression of the magnitude of the raw bearing measurement error. The time constant should be set to respond more quickly than the nominal response speed for the controller that regulates formation rotation angle; greater than an order of magnitude suppression of bearing measurement errors might be possible if the time constant or sample frequency can be further increased.

C. Simulation Results

This section describes simulation results for the IAP algorithm and the CMAP algorithm, both with and without post-processing. As a general observation, relative positioning errors shrink with increasing algorithm complexity, with errors growing smaller moving from IAP to CMAP, and from baseline CMAP to CMAP with post-processing. Results from representative Monte Carlo simulation are illustrated in Fig. 5 through Fig. 7. The three figures shows Monte Carlo position estimates for follower aircraft (AC2, AC3, and AC4), given that bearing measurement accuracy has a standard deviation of 1°. In the case of Fig. 5, results are computed using IAP; of Fig. 6, using the baseline CMAP algorithm; and of Fig. 7, using CMAP with post-processing. Monte Carlo estimates of follower position are plotted as light gray dots. The actual position of each follower is plotted as an open circle. The location of the lead aircraft is plotted as a circled cross.

The figures indicate that the dominant measurement errors for these simulations were bearing errors. The distribution of the Monte Carlo trials is expected to be approximately elliptical. As indicated by the figures, these ellipses are degenerate, with much greater extent in the cross-track direction (aligned with the North-South axis in this simulation) than the in-track direction (aligned with the East-West axis in this simulation). Whereas ranging errors affect relative position estimation along the vectors between aircraft, bearing errors effect estimation of

relative position in the perpendicular direction. Hence, it can be inferred that bearing errors dominate over ranging errors given the formation geometry and error models considered.

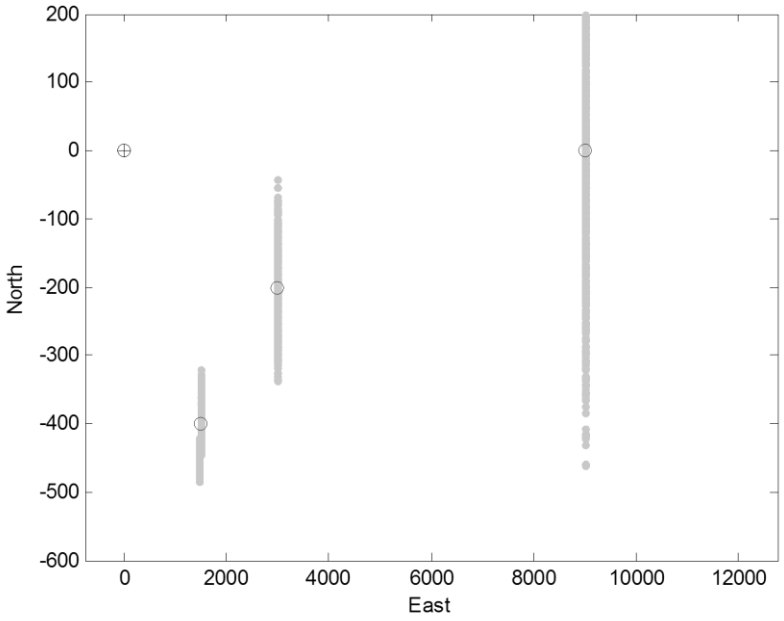

Fig. 5. Monte Carlo Simulation for IAP with Bearing Error Standard Deviation of 1°

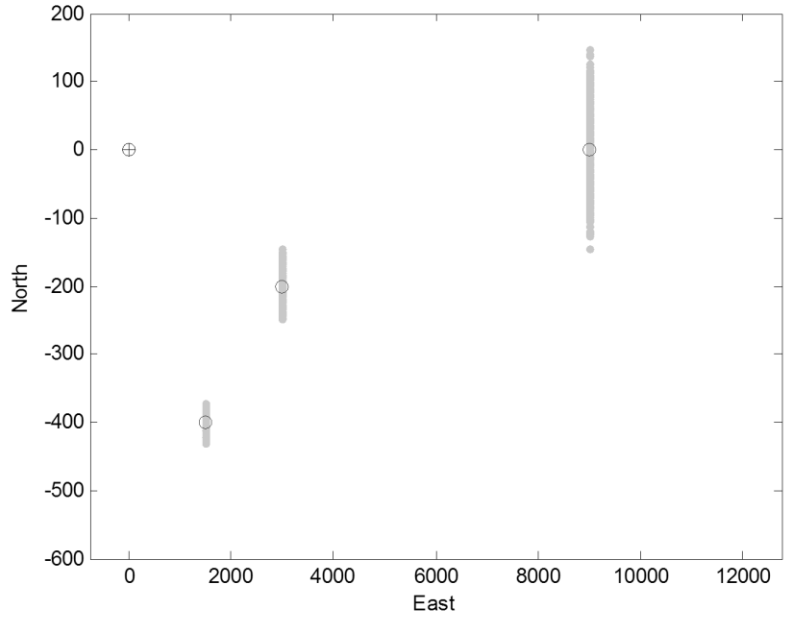

Fig. 6. Monte Carlo Simulation for Baseline CMAP with Bearing Error Standard Deviation of 1°

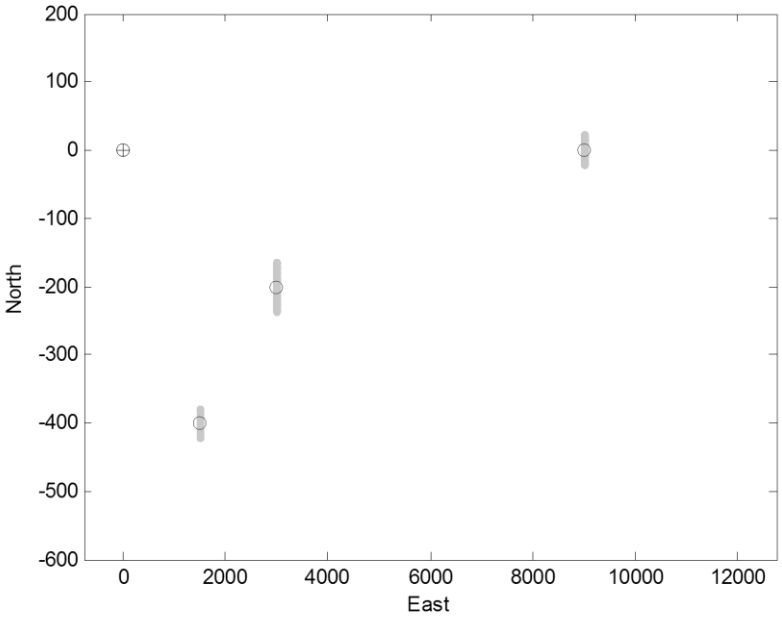

Fig. 7. Monte Carlo Simulation for CMAP with Post Processing for 1° Bearing Error

Additional Monte Carlo simulations were executed for a number of bearing error magnitudes (seven cases over the range of σ_α between 0.1° and 30°). In each scenario, error statistics were evaluated for 1000 trials, each with

different, randomly sampled measurement error values. Using these simulations, the in-track and cross-track relative positioning errors for each follower aircraft were analyzed to compute standard deviations. These statistical values for position-estimation standard deviation are plotted in Fig. 8 through Fig. 10, as a function of the assumed magnitude of bearing measurement errors. For comparison, relative-position standard deviation values obtained analytically, by linearization analysis, are also plotted. Results for IAP are shown in Fig. 8, for baseline CMAP in Fig. 9, and for CMAP with post-processing in Fig. 10.

In each figure, three curves are plotted, one for each follower. Square markers are used to indicate AC2. Circular markers indicate AC3. Triangular markers indicate AC4. Statistical (Monte Carlo) results are plotted as open markers, connected by straight lines. Probabilistic (linear analysis) results are plotted using smaller, closed markers. The scale of the horizontal and vertical axes is the same for all three figures.

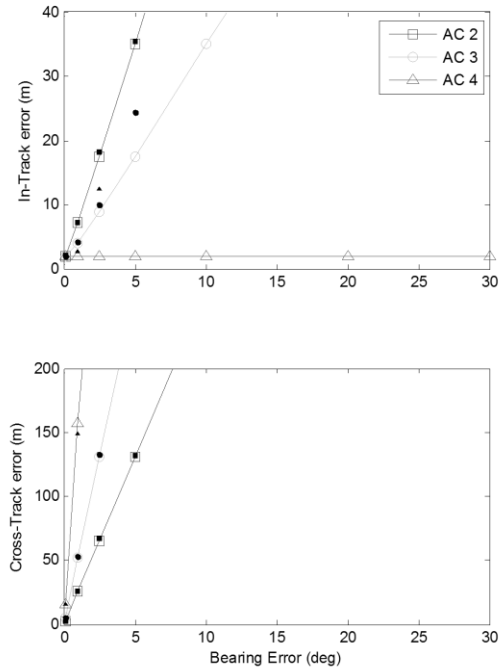

Fig. 8. Position Error Standard Deviations for IAP

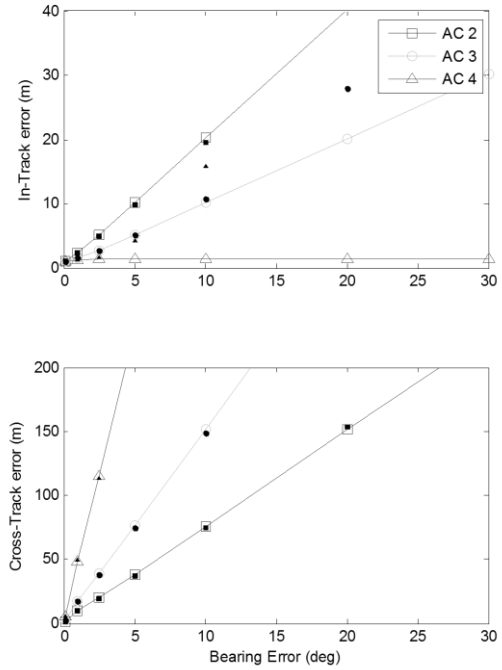

Fig. 9. Position Error Standard Deviations for baseline CMAP

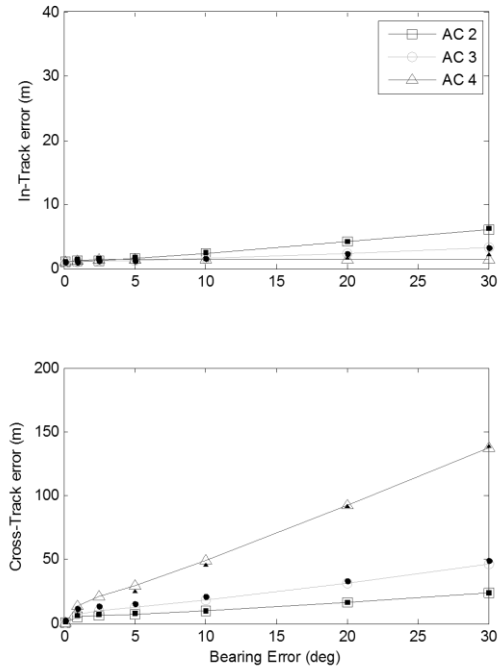

Fig. 10. Position Error Standard Deviations for CMAP with Post-Processing

Vertical error is not plotted, but in all cases, the vertical relative-positioning errors were essentially the same (about 14 m, one-sigma). This error level is equivalent to that of the difference between two altimeter measurements ($\sqrt{2}\sigma_a$ for independent Gaussian errors), indicating that the IAP and CMAP methods did little to improve the estimation of vertical position. This behavior is unsurprising because the simulated aircraft all flew at the same altitude. For such a formation, ranging and bearing measurements are perpendicular to the vertical direction, so vertical relative positioning information is extracted solely from altimeter data.

D. Discussion

In broad terms, the structure of the error plots for all three algorithms is similar. In all cases, the in-track error is smaller than the cross-track error. The primary reason for this difference is that the formation has a high aspect ratio, with aircraft spaced at long distances in the along-track direction and short distances in the cross-track direction. As such, high accuracy ranging measurements are aligned primarily with the in-track direction. Lower accuracy bearing measurements influence the perpendicular (cross-track) direction. Cross-track errors are quite sensitive to bearing measurement uncertainty. At 9000 m, the distance between AC1 and AC4, even a 1° bearing error results in a cross-track position error of 157 m. For CMAP, ranging measurements nonetheless provide significant information about cross-track spacing, despite the formation's long aspect ratio. These benefits are largely obscured in Fig. 5 through Fig. 10 because of uncertainty in the global rotation angle for the entire formation. Cross-track relative positioning accuracy would be significantly higher for CMAP, on the order of ranging measurement accuracy, were it not for this global rotation uncertainty.

To compare relative positioning algorithms more quantitatively, it is useful to consider an application-specific maximum-tolerable error bound. As mentioned in the introduction, the maximum tolerable cross-track positioning error for precision airdrop is approximately 50 m. The maximum-tolerable error bound will be defined as the one-sigma bearing value for which the one-sigma cross-track positioning error reaches 50 m. For the purposes of this paper, we will evaluate this condition for AC4, which is both a follower of AC1 and the leader for the second formation element.

Using this maximum-tolerable error criterion, it is possible to determine what levels of bearing-measurement error are acceptable for each algorithm considered. For IAP, the cross-track error bound is exceeded for a bearing

error standard deviation larger than 0.31°. For the baseline CMAP algorithm, the bound is exceeded for a bearing error standard deviation larger than 1.0°. Finally, for CMAP with post-processing (assuming τ/T equal to 100), the bound is exceeded for a bearing error standard deviation above 10.2°. Based on this analysis, CMAP provides about a factor of three greater tolerance to bearing measurement errors than IAP. (Marginal additional benefit could be obtained by processing CMAP for a formation with more than four aircraft.) Greater gains are possible by introducing post-processing, which makes CMAP about a factor of ten times more tolerant of bearing measurement errors than baseline CMAP without post-processing. The dramatic benefits of post-processing are indicative both of the underlying accuracy of CMAP and of its inherent ambiguity due to global rotation angle uncertainty. Once formation-rotation angle uncertainty is mitigated (for instance through post-processing), the benefits of CMAP are more readily apparent.

As noted previously, comparing probabilistic standard deviations (open markers) to statistically computed standard deviations (closed markers) aids in verifying the simulations results. In fact, the probabilistic and statistical computations generally agree very well. Agreement is particularly good when bearing-measurement error is low, as this is where the linearization used to obtain theoretical covariance matrices is most accurate. At larger levels of bearing-measurement error, theoretical and statistically computed standard deviations do diverge, especially for the IAP and baseline CMAP algorithms (Fig. 8 and Fig. 9, respectively). The divergence is largely due to the curvature of the actual error distribution, as large bearing errors arc around a circle of approximately constant radius. This motion around a circular radius for larger bearing errors causes cross-track errors to be somewhat lower than predicted by linear analysis and in-track errors to be somewhat higher.

It is perhaps surprising that the CMAP method with post-processing actually converges toward the linearized error model as bearing-measurement error increases. Fig. 10 shows that the theoretical prediction is reasonable (but slightly conservative) for bearing error standard deviation below 10°. The match between statistical and probabilistic analyses is very close above 10°, however. In fact, this observation corresponds well to the assumptions made regarding error modeling for CMAP with post-processing. In Section V.B, it was hypothesized that basic CMAP processing depended primarily on ranging measurement error and that post-processing depended primarily on bearing measurement error; the decoupled model was expected to become increasingly accurate as bearing measurement errors increased in magnitude. The fact that Monte Carlo simulations match the resulting linearization analysis at large bearing-angle magnitudes supports this hypothesis.

Ultimately, the choice of which algorithm is most appropriate for a particular formation-flight application depends not only on system accuracy but also on many secondary factors. Thus, even though CMAP achieves a higher accuracy than IAP, it may not be as desirable, both because IAP is much less complex to implement and because IAP requires no communication among aircraft in the formation. By comparison, implementing CMAP requires the solution of a linear algebra problem to obtain all the states in the state vector; furthermore, CMAP requires that measurement data be broadcast over a communication channel, possibly one that is superimposed on the navigation signal or possibly a supplementary channel. Furthermore, broadcast delays associated with this communication channel may introduce latency into the CMAP solution. Thus, practical issues of complexity, data communication and latency are important topics for future research.

VI. Conclusion

This paper introduced a new algorithm for collaborative relative positioning in formation-flight applications. The new algorithm, called Collaborative Multi-Aircraft Positioning (CMAP), fuses slant range, planar bearing and altimetry measurements from a team of aircraft to enhance positioning accuracy and enable time-of-flight measurements to be made without explicit synchronization of timing references on board each aircraft. The CMAP algorithm was compared to a more conventional algorithm that computes relative positions for each aircraft independently. Monte Carlo simulations were employed to compare the accuracy of the collaborative approach to a more conventional Independent Aircraft Positioning (IAP) approach. Simulations indicated that, all else equal, the CMAP algorithm was approximately three times more accurate in estimating relative positions between aircraft than IAP, at least in the direction which most limits performance for precision airdrop applications (e.g. the cross-track direction).

The major factor that limits CMAP accuracy is uncertainty in the estimation of the rigid-body rotation angle for the full formation (relative to North). To compensate for this limitation, a modified form of the CMAP algorithm was proposed. This modification introduced post-processing to smooth the estimate of the formation rotation angle. The result was a modified form of CMAP capable of providing instantaneous (“snapshot”) estimates of formation shape as well as filtered, slightly lagging estimates of the global formation-rotation angle. Simulations demonstrated that this form of CMAP with post-processing was an order of magnitude more accurate than the baseline CMAP algorithm and approximately 30 times more accurate than IAP.

VII. Acknowledgments

Thanks to AFRL (Contract FA8650-11-M-3117) and prime contractor Physics, Materials, and Applied Mathematics, Inc. for supporting this work.

VIII. References

[1] Blake, W., "Development of the C-17 Formation Airdrop Element Geometry," *Journal of Aircraft*, Vol. 35, No. 2, 1988, pp. 175-182.

[2] Blake, W., and Gingras, D., "Comparison of Predicted and Measured Formation Flight Interference Effects," *Journal of Aircraft*, Vol. 41, No. 2, 2004, pp. 201-207.

[3] Bower, G., Flanzer, T., and Kroo, I., "Formation Geometries and Route Optimization for Commercial Formation Flight," *AIAA Applied Aerodynamics Conference*, AIAA, San Antonio, TX, 2009.

[4] Ning, S., Flanzer, T., and Kroo, I., "Aerodynamic Performance of Extended Formation Flight," *Journal of Aircraft*, Vol. 48, No. 3, 2011, pp. 855-865.

[5] Khanafseh, S., and Pervan, B., "Autonomous Airborne Refueling of Unmanned Air Vehicles Using the Global Positioning System," *Journal of Aircraft*, Vol. 44, No. 5, 2007, pp. 1670-1682.

[6] Williamson, W., Glenn, G., Dang, V., Speyer, J., Stecko, S., and Takacs, J., "Sensor Fusion Applied to Autonomous Aerial Refueling," *Journal of Guidance, Control, and Dynamics*, Vol. 32, No. 1, 2009, pp. 262-275.

[7] Mobility Airlift Command, "C130 Operator's Guide to the SKE/ZM Air Delivery System," URL: http://gouge.mabrooks.com/SKE/MAC_PAMPHLET_55-43.doc [cited 09 July 2011].

[8] Beaubien, S., "Rethinking Strategic Brigade Airdrop," Master of Mobility Dissertation, Graduate School of Logistics and Acquisition Management, Air Force Institute of Technology, Wright Patterson Air Force Base, OH, 1997.

[9] Rivas, P., "Military Unique Applications of ADS-B," RTCA SC-186, Working Group 6, Meeting 4, URL: http://adsb.tc.faa.gov/WG6_Meetings/Meeting4/242A-WP-4-10%20Military%20Apps.pdf [cited 09 July 2011].

[10] Doane, P., U.S. Patent for "Autonomous Station Keeping System for Formation Flight," U.S. 7024309, issued on 4 Apr. 2006.

[11] Williamson, W., Rios, T., and Speyer, J., "Carrier Phase Differential GPS/INS Positioning for Formation Flight," American Control Conference (ACC), San Diego, CA, 1999.

[12] Haissig, "Military Formation Flight as a Model for Increased Capacity in Civilian Airspace," *Digital Avionics Systems Conference (DASC)*, IEEE, Salt Lake City, UT, 2004.

[13] Williamson, W. Abdel-Hafez, M., Rhee, I., Song, E.-J., Wolfe, J., Chichka, D., and Speyer, J., "An Instrumentation System Applied to Formation Flight," *IEEE Transactions on Control Systems Technology*, Vol. 15, No. 1, 2007, pp. 75-85.

[14] John A. Volpe National Transportation Systems Center, "Vulnerability Assessment of the Transportation Infrastructure Relying on the Global Positioning System," 29 Aug. 2001.

[15] Rife, J., Khanafseh, S., Pullen, S., De Lorenzo, D., Ung-Suok Kim, Koenig, M., Tsung-Yu Chiou, Kempny, B., and Pervan, B., "Navigation, Interference Suppression, and Fault Monitoring in the Sea-Based Joint Precision Approach and Landing System," *Proc. of the IEEE*, vol. 96, no. 12, 2008, pp. 1958 – 1975.

[16] Nishino, H., Tateishi, K., Ikegami, T., "Inter-Satellite Location Measurement of the Formation Flight Satellite System using UWB signal," *AIAA International Communications Satellite Systems Conference*, AIAA, Seoul, South Korea, 2007.

[17] Tahk, M.-J., Park, C.-S., Ryoo, C.-K., "Line-of-Sight Guidance Laws for Formation Flight," *Journal of Guidance, Control, and Dynamics*, Vol. 28, No. 4, 2005, pp. 708-716.

[18] Fosbury, A., and Crassidis, J., "Relative Navigation of Air Vehicles," *Journal of Guidance, Control, and Dynamics*, Vol. 31, No. 4, 2008, pp. 824-834.

[19] Anderle, M., Crassidis, J., Linares, R., Cheng, Y., and Hyun, B., "Deterministic Relative Attitude Determination of Three-Vehicle Formations," *Journal of Guidance, Control, and Dynamics*, Vol. 32, No. 4, 2009, pp. 1077-1088.

[20] Chen, T., and Xu, S., "Approach Guidance with Double-Line-of-Sight-Measuring Navigation Constraint for Autonomous Rendezvous," *Journal of Guidance, Control, and Dynamics*, Vol. 34, No. 3, 2011, pp. 678-687.

[21] Giulietti, F., Innocenti, M., Pollini, L., "Sensorless Formation Flight," *AIAA Guidance, Navigation, and Control Conference and Exhibition*, AIAA, Montreal, Canada, 2001.

[22] Simon, D., *Optimal State Estimation: Kalman, H_∞ and Nonlinear approaches*, Wiley, Hoboken, NJ, 2006.

[23] Misra, P., and Enge, P., *Global Positioning System: Signals, Measurements and Performance, Revised 2nd Ed.*, Ganga-Jamuna Press, Lincoln, MA, 2011.